



This is a repository copy of *Computationally efficient 3D analytical magnet loss prediction in surface mounted permanent magnet machines.*

White Rose Research Online URL for this paper:  
<http://eprints.whiterose.ac.uk/109772/>

Version: Accepted Version

---

**Article:**

Nair, S.S., Chen, L., Wang, J. [orcid.org/0000-0003-4870-3744](https://orcid.org/0000-0003-4870-3744) et al. (3 more authors)  
(2017) Computationally efficient 3D analytical magnet loss prediction in surface mounted permanent magnet machines. IET Electric Power Applications, 11 (1). pp. 9-18. ISSN 1751-8660

<https://doi.org/10.1049/iet-epa.2016.0079>

---

**Reuse**

Unless indicated otherwise, fulltext items are protected by copyright with all rights reserved. The copyright exception in section 29 of the Copyright, Designs and Patents Act 1988 allows the making of a single copy solely for the purpose of non-commercial research or private study within the limits of fair dealing. The publisher or other rights-holder may allow further reproduction and re-use of this version - refer to the White Rose Research Online record for this item. Where records identify the publisher as the copyright holder, users can verify any specific terms of use on the publisher's website.

**Takedown**

If you consider content in White Rose Research Online to be in breach of UK law, please notify us by emailing [eprints@whiterose.ac.uk](mailto:eprints@whiterose.ac.uk) including the URL of the record and the reason for the withdrawal request.



[eprints@whiterose.ac.uk](mailto:eprints@whiterose.ac.uk)  
<https://eprints.whiterose.ac.uk/>

# Computationally Efficient 3D Analytical Magnet Loss Prediction in SPM Machines

Sreeju S Nair<sup>1\*</sup>, Liang Chen<sup>1</sup>, Jiabin Wang<sup>1</sup>, Robert Chin<sup>2</sup>, Iakovos Manolas<sup>2</sup>, Dmitry Svehkarenko<sup>2</sup>

<sup>1</sup> Department of Electronic and Electrical Engineering, The University of Sheffield, S1 3JD, United Kingdom

<sup>2</sup> ABB Corporate Research, SE-721 78 Västerås, Sweden

\* [ssnair1@sheffield.ac.uk](mailto:ssnair1@sheffield.ac.uk)

**Abstract:** This paper proposes a computationally efficient analytical method, for accurate prediction of 3-dimensional (3D) eddy current loss in the rotor magnets of surface mounted permanent magnet machines considering slotting effect. Sub-domain model incorporating stator tooth tips is employed to generate the information on radial and tangential time-derivatives of 2D magnetic field (eddy current sources) within the magnet. The distribution of the eddy current sources in 3D is established for the magnets by applying the eddy current boundary conditions and the Coulomb gauge imposed on the current vector potential. The 3D eddy current distributions in magnets are derived analytically by employing the method of variable separation and the total eddy current loss in the magnets are subsequently established. The method is validated by 3D time-stepped finite element analysis (FEA) for 18-slot, 8-pole and 12-slot, 8-pole permanent magnet machines. The eddy current loss variations in the rotor magnets with axial and circumferential numbers of segmentations are studied. The reduction of magnet eddy current loss is investigated with respect to harmonic wavelength of the source components to suggest a suitable segmentation for the rotor magnets in SPM machines.

## 1. Introduction

High power density surface mounted permanent magnet (SPM) machines [1] with modular winding configuration [2, 3] generates a large amount of MMF space harmonics rotating in forward and backward directions. These harmonics, coupled with slotting and supply time harmonics can produce increased eddy current loss in magnets especially when operating at higher speeds. Hence such machines employing highly conductive Nd-Fe-B magnets may suffer from elevated temperature rise that will increase the risk of partial demagnetization [4]. Axial and circumferential segmentation of the magnets are often employed to reduce these losses [5]. An accurate prediction of magnet loss at the design stage, not only give a better efficiency evaluation, but also may prevent excessive temperature rise in magnets and hence reduce the risk of partial demagnetization.

In order to evaluate and analyse the eddy current losses [6] in the magnets, variety of methods have been reported in a large number in literatures. In general, evaluation of rotor eddy current losses requires simultaneous solutions for the governing equations of the magnetic and eddy current fields. The computationally efficient 2D numerical methods such as transient FEA to calculate the eddy current losses

[7-9], can yield good results but lacks any physical insight on the mechanism of eddy current loss. Hence a few 2D analytical methods are developed to predict the magnet eddy current loss with varying degree of accuracy [10-16]. The reduction in magnet loss with circumferential segmentations can be successfully evaluated using these methods. However, they ignore the slotting effect and approximates winding currents by an equivalent current sheet distributed over the stator bore radius. The method of choosing a suitable pole –slot combination for minimizing the rotor loss in permanent magnet machines is described in [17, 18].

Unless the slotting harmonics are considered in the loss evaluation, the no load magnetic loss and also its interaction with the armature field harmonics at diverse load conditions cannot be quantified [19]. As the eddy current density inside the magnet is evaluated from the time derivative of the magnetic vector potential within it, a sufficiently accurate machine model which accounts the slotting effect becomes indispensable to estimate these time variations. Magnet loss evaluation employing 2D relative permeance model [20-22] gives a better estimation of no-load magnet losses, but the results deviate from the actual values when the loss due to armature reaction is considered. While improved flux density assessment models are proposed in [23-25] by employing complex relative permeability to predict magnet loss [26], a better accurate subdomain models [27-29] are preferred for loss estimation in permanent magnets [19, 30]. These methods except [11], [21] [22] and [26] are mainly resistance limited assuming the skin depth for the eddy currents is sufficiently high under the normal operating conditions of the machine.

While 2D evaluation of eddy current loss in SPM machines can be performed analytically considering slotting effect, its accuracy is compromised if the axial length of magnets is comparable to their other dimensions since the eddy current flow in the magnets may become predominantly 3-dimensional (3D). In order to overcome the enormous computation time in magnet loss evaluation encountered in 3D FEA, computationally efficient reduced order numerical methods and 3D analytical methods have received significant interest in research communities [31-39]. These reduced order numerical methods may be computationally efficient, however are complicated to implement. Also, the 3D analytical methods reported for SPMs, ignores slotting effect and the radial variation of flux density along the magnets. Most of these methods also discard the field produced by the permanent magnets and the loss contribution by the tangential component of the magnetic field. Moreover, these methods also ignore the variation of loss among different magnet segments in computing the total eddy current loss. The 3D eddy current loss model for magnets published in [40] considering only machines with narrow slot openings using Carter's theory fails to replicate the flux density undulations accurately. Inaccurate eddy current loss calculation may cause underestimation of rotor temperatures, which in turn increases demagnetization risk.

Therefore, an accurate and computationally-efficient solution for quantifying the eddy current losses is necessary.

The method of generalized imaging is proposed in [41] to establish the eddy current source distribution in the form of 3D Fourier series in  $x, y, z$  directions. Ultimately only the coefficients for the sines and cosines needed to be evaluated using Fourier expansion in three dimensions. While the physical concept for the images is clear, the mathematical process to represent the sources and images in 3D space is quite cumbersome. Also the slotting effect is not included in [41] and hence cannot be used to predict the 3D no-load magnet loss, and to assess the effect of slotting under load conditions. The method of magnet eddy current loss prediction accounting eddy current reaction is proposed in [42] employing the magnetic field variations from 2D FEA. However, this method cannot be employed for predicting the 3D magnet loss associated with different harmonic components with increase in axial and circumferential segmentations.

This paper establishes the 3D eddy current source distributions in a much more elegant manner. The rest of the paper is organized as follows. Section 2 derives 2D eddy current source distribution from the sub-domain model. Section 3 describes the governing equations and boundary conditions for 3D eddy current field. Section 4 establishes the radial and tangential source distributions in 3D based on the boundary conditions for the eddy current density and the Coulomb gauge adopted for the current vector potential. Section 5 validates the proposed method on 18-slot, 8-pole and 12-slot, 8-pole SPM machines by evaluating its magnet loss with due account of slotting at no load and at peak load conditions and comparing the results with time-stepped 3D FEA. In section 6 the significance of the source components in loss evaluation is established and the loss associated with different source harmonics with increase in number of segmentations is quantified to study the relationship between harmonic wavelength and the segment width in magnet loss reduction. Section 7 summarizes the findings in conclusion.

## 2. Sub domain model and calculation of magnet flux density variation

The subdomain model with simplified slots and uniform distribution of current in them is presented by assuming infinitely permeable iron materials and it replicates the flux density variations in the magnet quiet accurately [29]. The radial and tangential component of the flux density at a radius 'r' along the magnet, which contributes to the magnet loss can be represented in the rotor reference as,

$$B_r = \sum_k [-C_k A_1 \sin(k\theta_r + k\omega_r t) + C_k C_1 \cos(k\theta_r + k\omega_r t)] \quad (1)$$

$$B_t = \sum_k [-D_k A_1 \cos(k\theta_r + k\omega_r t) - D_k C_1 \sin(k\theta_r + k\omega_r t)] \quad (2)$$

where  $C_k = k/r C_{1k}$ ,  $D_k = -1/r C_{4k}$ ,  $\theta_r$  and  $\omega_r$  are rotor position and angular speed, respectively. The coefficients which accounts for the slotting effect,  $A_1$  and  $C_1$ , varies with rotor position and can be expressed as Fourier series:

$$A_1 = \sum_l a_{1l} \cos(lp\omega_r t + \psi_{al}) \quad (3)$$

$$C_1 = \sum_l c_{1l} \cos(lp\omega_r t + \psi_{cl}) \quad (4)$$

where  $l=1, 2, 3 \dots$  and  $p$  is the number of pole pairs.

The  $\partial B_r / \partial t$  and  $\partial B_t / \partial t$  calculated from (1) to (4) form the source for eddy current generation in the magnets and they are given by,

$$\frac{\partial B_r}{\partial t} = \sum_k \sum_l C_k \left[ \begin{array}{l} a_{br} (k + lp)\omega_r \cos(k\theta_r + (k + lp)\omega_r t + \psi_{br}) \\ + a_{fr} (k - lp)\omega_r \cos(k\theta_r + (k - lp)\omega_r t + \psi_{fr}) \end{array} \right] \quad (5)$$

$$\frac{\partial B_t}{\partial t} = \sum_k \sum_l D_k \left[ \begin{array}{l} a_{b\alpha} (k + lp)\omega_r \cos(k\theta_r + (k + lp)\omega_r t + \psi_{b\alpha}) \\ + a_{f\alpha} (k - lp)\omega_r \cos(k\theta_r + (k - lp)\omega_r t + \psi_{f\alpha}) \end{array} \right] \quad (6)$$

The expressions for  $a_{br}$ ,  $a_{fr}$ ,  $\psi_{br}$ ,  $\psi_{fr}$ ,  $a_{b\alpha}$ ,  $a_{f\alpha}$ ,  $\psi_{b\alpha}$ ,  $\psi_{f\alpha}$ , are defined in Appendix 9.1. The first term in the square bracket in (5) and (6) is associated with backwards rotating harmonics and the second term with forward rotating harmonics. Separation of magnetic field variations as forward and backward rotating harmonics helps in separating the losses associated with different harmonics. The definitions for other coefficients in (1)-(6) can be found in [29].

### 3. Field description for eddy currents in rectangular magnets

From Faraday's induction law and neglecting eddy current reaction, the eddy current density distribution  $J$  in magnets at a given time instant is dependent on the rate of change of flux density  $B$  with time which can be seen as a source distribution denoted by  $S$ . Their relation is expressed as (7).

$$\begin{aligned} \nabla \times J &= \sigma S \\ S_x &= -\frac{\partial B_x}{\partial t}, S_y = -\frac{\partial B_y}{\partial t}, S_z = -\frac{\partial B_z}{\partial t} \end{aligned} \quad (7)$$

where  $\sigma$  is the conductivity of magnets. According to the continuity law of the eddy current density,  $\nabla \cdot J = 0$ ,  $J$  may be expressed as the curl of a current vector potential  $A$  in ( 8).

$$\nabla \times A = J$$

8)

Applying the Coulomb gauge  $\nabla \cdot A = 0$ , it can be shown that the current vector potential  $A$  satisfies:

$$\nabla^2 A = -\sigma S$$

(9)

Fig.1a indicates a magnet in a SPM machine in which the eddy current field is induced by 2D time-varying magnetic field. The magnet is approximated in rectangular shape by neglecting its curvature effect. The circumferential direction is denoted as  $x$ , radial direction as  $y$  and axial direction as  $z$ . It is assumed that the magnetic field distribution in the machine is two-dimensional, and hence the flux density has  $x$  and  $y$  components which is independent of  $z$ . Thus, the source vector  $S$  only has two components  $S_x = \partial B_x / \partial t$  and  $S_y = \partial B_y / \partial t$ . The dimensions of the magnets in the three directions are denoted as  $L_x$ ,  $L_y$  and  $L_z$  respectively.

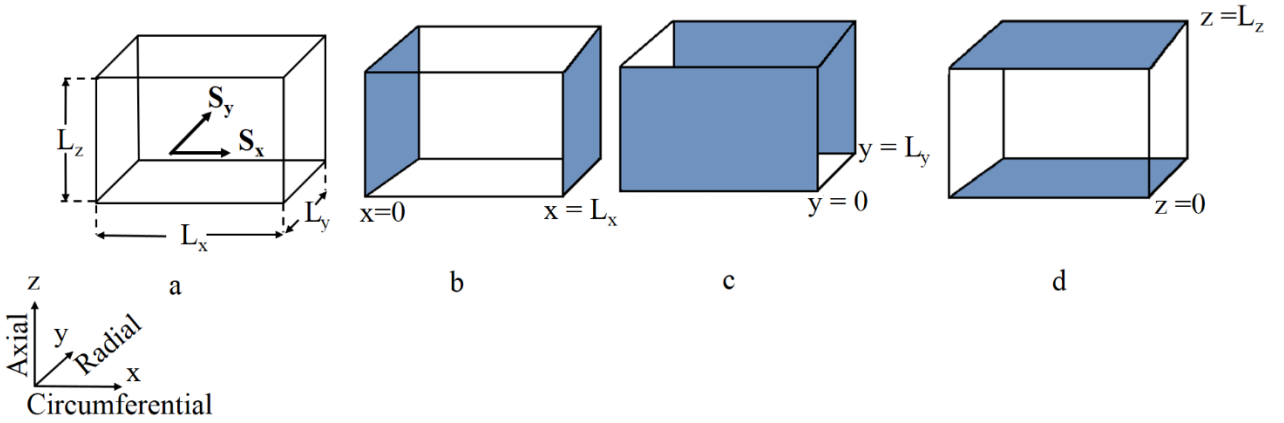


**Fig.1.** A rectangular magnet in a SPM machine indicating its six surfaces with eddy current field excited by 2D magnetic field  
a Magnet dimensions and source fields  
b Magnet surfaces  $x = 0$  and  $x = L_x$   
c Magnet surfaces  $y = 0$  and  $y = L_y$   
d Magnet surfaces  $z = 0$  and  $z = L_z$

Since the conductivity outside the magnet is zero, the boundary conditions on the six magnet surfaces, namely, two parallel  $x$ - $z$  planes, two  $y$ - $z$  planes and two  $x$ - $y$  planes, are given by:

$$n_v \cdot J = 0$$

(

10)

where  $n_v$  denotes the normal vectors of the magnet surfaces.

#### 4. Solution to 3D source distribution from the boundary conditions for a rectangular magnet

At a given rotor position, the source distributions,  $S_x$  and  $S_y$  in a rotor magnet are known and may be expanded into 3D space by 3D Fourier series of the following form:

$$S_x = \sum_{m=1}^{\infty} \sum_{n=1}^{\infty} \sum_{k=1}^{\infty} a_{(m,n,k)} \cos(mP_{x_1}x + \psi_{x_1}) \cos(nP_{y_1}y + \psi_{y_1}) \cos(kP_{z_1}z + \psi_{z_1}) \quad (11)$$

$$S_y = \sum_{m=1}^{\infty} \sum_{n=1}^{\infty} \sum_{k=1}^{\infty} b_{(m,n,k)} \cos(mP_{x_2}x + \psi_{x_2}) \cos(nP_{y_2}y + \psi_{y_2}) \cos(kP_{z_2}z + \psi_{z_2}) \quad (12)$$

where  $m, n, k$  are the harmonic orders in  $x, y, z$  directions respectively.  $P_{x_1}, P_{y_1}, P_{z_1}, P_{x_2}, P_{y_2}, P_{z_2}$  and the phase angles  $\psi_{x_1}, \psi_{y_1}, \psi_{z_1}, \psi_{x_2}, \psi_{y_2}, \psi_{z_2}$  are the parameters to be determined in order to satisfy the physical constraints of eddy current distributions.

The 3D Fourier expansion implies that the source distribution within the magnets is repeated periodically in 3D space although the space of the concern is limited within the magnet defined by its dimensions  $L_x, L_y$  and  $L_z$ . The solutions of the current vector potential  $A_x, A_y$  which satisfy Poisson's equation of (9) with the source  $S_x, S_y$  distribution in (11) and (12) are given by:

$$A_x = \sum_{m=1}^{\infty} \sum_{n=1}^{\infty} \sum_{k=1}^{\infty} c_{(m,n,k)} \cos(mP_{x_1}x + \psi_{x_1}) \cos(nP_{y_1}y + \psi_{y_1}) \cos(kP_{z_1}z + \psi_{z_1}) \quad (13)$$

$$A_y = \sum_{m=1}^{\infty} \sum_{n=1}^{\infty} \sum_{k=1}^{\infty} d_{(m,n,k)} \cos(mP_{x_2}x + \psi_{x_2}) \cos(nP_{y_2}y + \psi_{y_2}) \cos(kP_{z_2}z + \psi_{z_2}) \quad (14)$$

where  $c_{(m,n,k)}$  and  $d_{(m,n,k)}$  are the coefficients associated with  $(n, m, k)$ th harmonic for the current vector potential. Consequently  $J_x, J_y, J_z$  can be derived from (8) as,

$$J_x = \sum_{m=1}^{\infty} \sum_{n=1}^{\infty} \sum_{k=1}^{\infty} e_{(m,n,k)} \cos(mP_{x_2}x + \psi_{x_2}) \cos(nP_{y_2}y + \psi_{y_2}) \sin(kP_{z_2}z + \psi_{z_2}) \quad (15)$$

$$J_y = \sum_{m=1}^{\infty} \sum_{n=1}^{\infty} \sum_{k=1}^{\infty} h_{(m,n,k)} \cos(mP_{x_1}x + \psi_{x_1}) \cos(nP_{y_1}y + \psi_{y_1}) \sin(kP_{z_1}z + \psi_{z_1}) \quad (16)$$

$$J_z = \sum_{m=1}^{\infty} \sum_{n=1}^{\infty} \sum_{k=1}^{\infty} q_{1(m,n,k)} \sin(mP_{x_2}x + \psi_{x_2}) \cos(nP_{y_2}y + \psi_{y_2}) \cos(kP_{z_2}z + \psi_{z_2}) + q_{2(m,n,k)} \cos(mP_{x_1}x + \psi_{x_1}) \sin(nP_{y_1}y + \psi_{y_1}) \cos(kP_{z_1}z + \psi_{z_1}) \quad (17)$$

where,  $e_{(m,n,k)}$ ,  $h_{(m,n,k)}$ ,  $q_{1(m,n,k)}$ , and  $q_{2(m,n,k)}$  are the coefficients associated with  $(n, m, k)^{\text{th}}$  harmonic for the eddy current densities which are derived from  $a_{(m,n,k)}$  and  $b_{(m,n,k)}$  after the operations defined in (8) and (9). From the boundary condition given in (10) the normal component of the current density need to be zero along all the six surfaces of the magnet as shown in Fig.1.

For the surfaced defined by  $x = 0$  and  $x = L_x$ , as shown in Fig.1b, the normal current density  $J_x = 0$ . From (15), it demands  $\cos(mP_{x_2}x + \psi_{x_2}) = 0$  at  $x = 0$  and  $x = L_x$ . Hence,  $P_{x_2} = \frac{\pi}{L_x}$  and  $\psi_{x_2} = \frac{\pi}{2}$ .

For the surface defined by  $y = 0$  and  $y = L_y$ , as shown in Fig.1c, the normal current density  $J_y = 0$ . From (16), it demands  $\cos(nP_{y_1}y + \psi_{y_1}) = 0$  at  $y = 0$  and  $y = L_y$ . Hence,  $P_{y_1} = \frac{\pi}{L_y}$  and  $\psi_{y_1} = \frac{\pi}{2}$ .

And finally for the face with  $z = 0$  and  $z = L_z$ , as shown in Fig.1d, the normal current density  $J_z = 0$ . From (17), it demands  $\cos(kP_{z_1}z + \psi_{z_1}) = 0$  and  $\cos(kP_{z_2}z + \psi_{z_2}) = 0$ , at  $z = 0$  and  $z = L_z$ . Hence,

$$P_{z_1} = \frac{\pi}{L_z} \text{ and } \psi_{z_1} = \frac{\pi}{2} \text{ also } P_{z_2} = \frac{\pi}{L_z} \text{ and } \psi_{z_2} = \frac{\pi}{2}.$$

Now from the Coulomb gauge  $\nabla \cdot A = 0$  imposed over the magnet volume, as the PM is insulated on all its surfaces it needs to be satisfied along all its surfaces too,

hence

$$\sum_{m=1}^{\infty} \sum_{n=1}^{\infty} \sum_{k=1}^{\infty} \left\{ c_{(m,n,k)}^1 \sin(mP_{x_1}x + \psi_{x_1}) \cos(nP_{y_1}y + \psi_{y_1}) \cos(kP_{z_1}z + \psi_{z_1}) \right. \\ \left. + d_{(m,n,k)}^1 \cos(mP_{x_2}x + \psi_{x_2}) \sin(nP_{y_2}y + \psi_{y_2}) \cos(kP_{z_2}z + \psi_{z_2}) \right\} = 0 \quad (18)$$

At  $x = 0$  and  $x = L_x$ , (18) demands  $\sin(nP_{x_1}x + \psi_{x_1}) = 0$ , which leads to  $P_{x_1} = \frac{\pi}{L_x}$  and  $\psi_{x_1} = 0$ .

Similarly, at  $y = 0$  and  $y = L_y$ , (18) demands  $\sin(nP_{y_2}x + \psi_{y_2}) = 0$ , hence  $P_{y_2} = \frac{\pi}{L_y}$  and  $\psi_{y_2} = 0$ .

Substituting  $P_{x_1}, P_{y_1}, P_{z_1}, P_{x_2}, P_{y_2}, P_{z_2}$  and the phase angles  $\psi_{x_1}, \psi_{y_1}, \psi_{z_1}, \psi_{x_2}, \psi_{y_2}, \psi_{z_2}$  into (11), (12) gives,

$$S_x = \sum_{m=1}^{\infty} \sum_{n=1}^{\infty} \sum_{k=1}^{\infty} a_{(m,n,k)} \cos\left(m \frac{\pi}{L_x} x\right) \sin\left(n \frac{\pi}{L_y} y\right) \sin\left(k \frac{\pi}{L_z} z\right) \quad (19)$$

$$S_y = \sum_{m=1}^{\infty} \sum_{n=1}^{\infty} \sum_{k=1}^{\infty} b_{(m,n,k)} \sin\left(m \frac{\pi}{L_x} x\right) \cos\left(n \frac{\pi}{L_y} y\right) \sin\left(k \frac{\pi}{L_z} z\right) \quad (20)$$

As proved using the generalized imaging technique in [41], it can be observed from (19) and (20) that across the normal boundary the sources has been mirrored, while it has become inverted mirror image across the tangential boundary. Hence the sources  $S_x, S_y$  can be observed to be repeating itself at every  $2L_x, 2L_y, 2L_z$ . This allows to compute the source frequency components within a magnet. The relation for the  $A_x, A_y, J_x, J_y$  and  $J_z$  can also be evaluated in the same manner after substitution. Once the eddy current distribution is known the total eddy current loss at a given time instant is the sum of the losses associated with each harmonic component:

$$\begin{aligned} P_{eddy} &= \sum_{m=1}^{\infty} \sum_{n=1}^{\infty} \sum_{k=1}^{\infty} P_{(m,n,k)} \\ &= \sum_{m=1}^{\infty} \sum_{n=1}^{\infty} \sum_{k=1}^{\infty} \frac{1}{8} \int_0^{2L_x} \int_0^{2L_y} \int_0^{2L_z} \frac{1}{\sigma} \cdot [J_{x(m,n,k)}^2 + J_{y(m,n,k)}^2 + J_{z(m,n,k)}^2] dx dy dz \\ &= \sum_{m=1}^{\infty} \sum_{n=1}^{\infty} \sum_{k=1}^{\infty} \{p_{1(m,n,k)} + p_{2(m,n,k)} + p_{3(m,n,k)} + p_{4(m,n,k)} + p_{5(m,n,k)}\} \end{aligned} \quad (21)$$

The coefficients,  $c(m,n,k), d(m,n,k), e(m,n,k), h(m,n,k), q(m,n,k)$  for the current vector potential and eddy current densities, and  $p_1(m,n,k) - p_5(m,n,k)$  for the total eddy current loss are all arithmetic functions of the harmonic order and magnet dimensions. They are summarized in Appendix 9.2. The process of implementation of the method is described in [41].

## 5. Finite element validation

### 5.1. Machine topology and design parameters

The proposed method is applied to 5kW 18-slot 8-pole and 12-slot,8-pole SPM machines for the evaluation of the eddy current loss in the rotor permanent magnets. The subdomain model [29] employed here can deal with both overlapping and non-overlapping type of double layer windings. The 18-slot 8-pole SPM machine considered uses an overlapping type of winding and the 12-slot,8-pole SPM machine employs a non-overlapping winding as shown in Figs.2a and b. The torque comparison at load conditions for both the machines is shown in Fig. 2c. The key physical parameters and specifications are listed in Table 1.

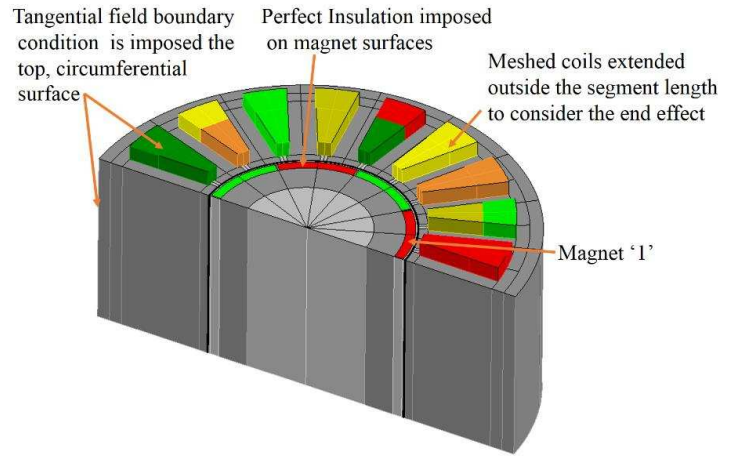
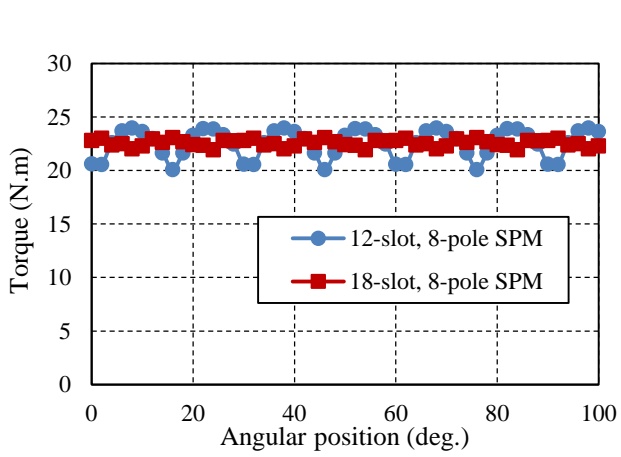
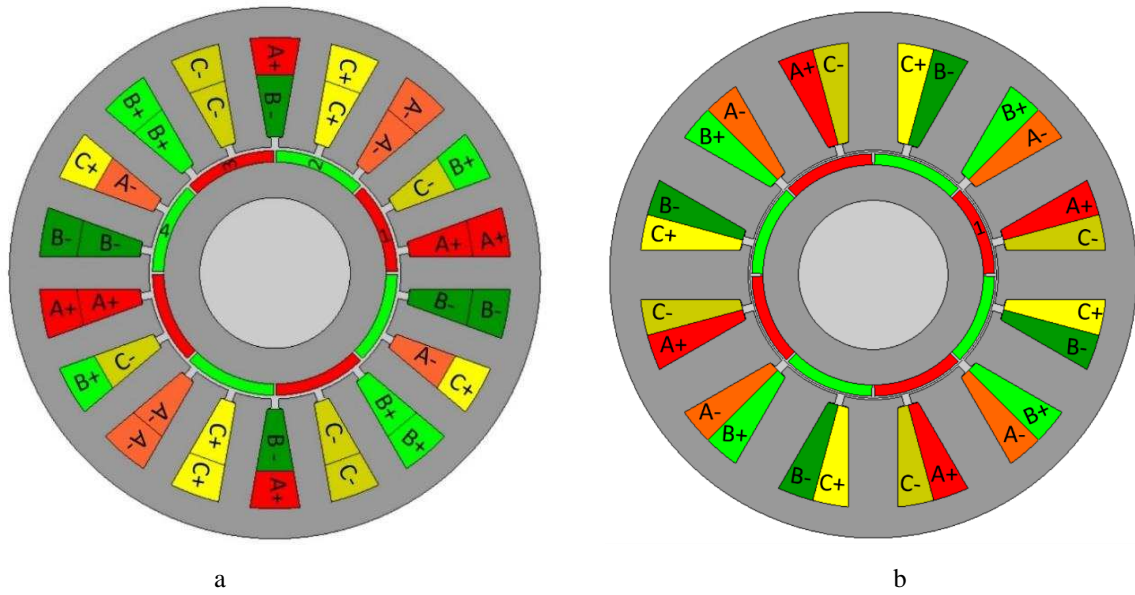


**Fig.2** SPM machine models and torque comparison

a 2D FE model -18-slot, 8-pole machine

b 2D FE model- 12 slot, 8-pole machine

c Torque comparison for both the machines at load conditions ( $I_d = 0A, I_q = 55A$  (peak) ,4500 rpm)

d 3D FE model- 18 slot, 8-pole machine

**TABLE 1** Key dimensions and specifications of the SPM machines

Parameter	Unit	18-slot, 8-pole	12-slot, 8-pole
Stator outer radius	mm	70.59	70.59
Motor stack length	mm	118	118

Rotor radius	mm	32.5	32.5
Magnet thickness	mm	3.0	3.0
Magnet pole arc	elec.deg	175	175
Slot opening	mm	2.03	2.03
Slot opening depth	mm	2.375	2.375
Slot depth	mm	29.15	29.15
Teeth width	mm	8.5	12.5
Shaft radius	mm	20.0	20.0
No. of turns/coil	No.	6	10
Magnet remanent flux density	T	1.1	1.1
Magnet resistivity	$\Omega.m$	$1.8 \times 10^{-6}$	$1.8 \times 10^{-6}$
Maximum speed	rpm	4500	4500
Rated current	A	39	39
Rated speed	rpm	2100	2100

### 5.2. 2D FE for field source validations

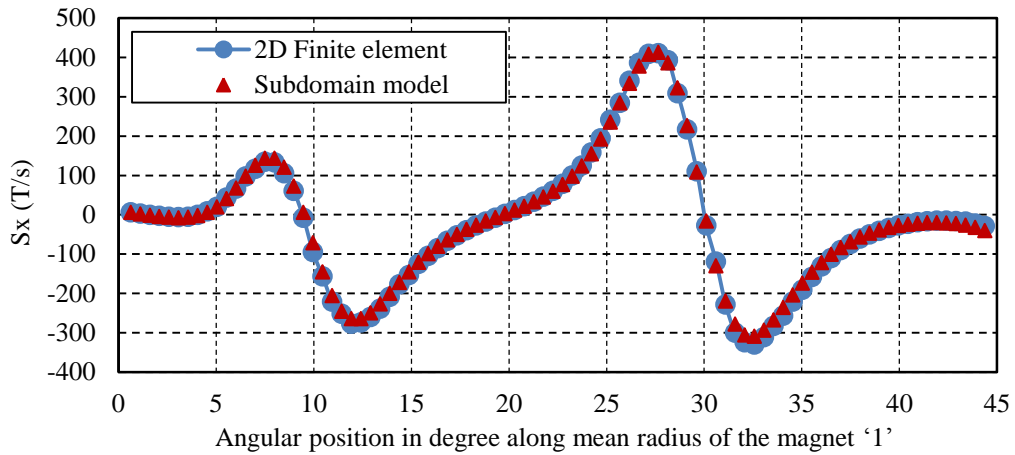
2D eddy current source field distributions considering slotting is obtained from the subdomain model, which neglects the magnetic saturation in the machine. Before proceeding to the eddy current calculations it is insightful to have a comparison for the magnetic field variation with the results obtained from 2D FEA. The eddy currents and the associated loss are evaluated when the machine is operated at peak load (peak phase current of 55A) at the maximum speed of 4500rpm.

Fig. 3 compares the analytically and 2D FE predicted eddy current source component variations with angular position at a given time instant of  $\omega_r t = 1.25^0$  (mech.) for the magnet '1' when the SPM machines operates at the load conditions mentioned before, where  $\omega_r$  is the fundamental electric angular frequency of the operation. It can be seen that the analytical predictions agree very well with those obtained from the 2D FEAs accounting material saturation. This ensures the accuracy of the source of excitation of the eddy current distribution to be analytically predicted by the proposed method.

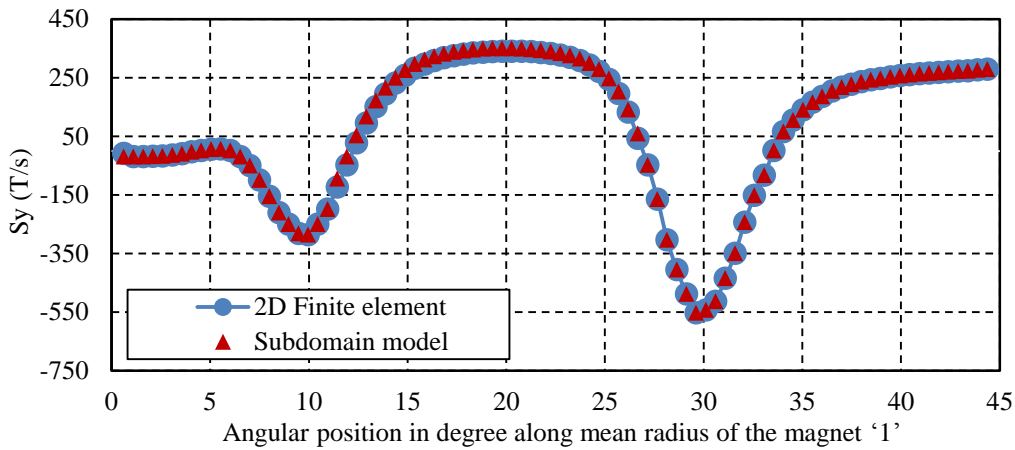
### 5.3. Comparisons of eddy current distribution and eddy current loss with 3D FEAs

A 3D FE model of the machine, as shown in Fig. 2d has been built to predict the 3D eddy current distribution and resultant eddy current loss induced in the magnets. Since the machine employs fractional slot per pole topology, circumferential symmetry exists only over 180 mechanical degrees. Thus, a quarter

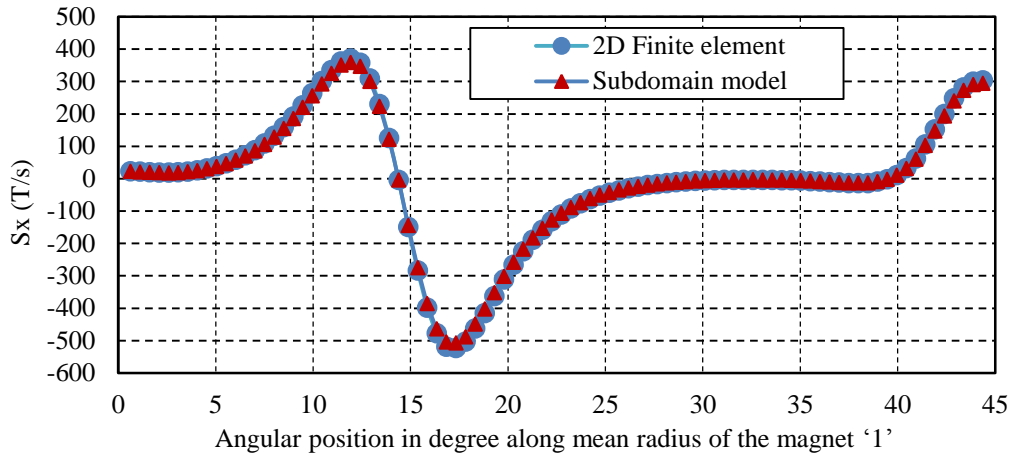
of the machine has to be modelled in 3D FEAs. The meshed coils are extended in the axial direction to consider the winding end effect. Tangential boundary conditions are imposed on this extended surface. A perfect insulation boundary conditions are applied to the axial and circumferential end surfaces of the magnets to insulate the segments from each other. In addition, the conductivity of the rotor iron core is not considered to avoid the eddy current flow in them. In practice, segmented pieces are glued together by high temperature epoxy which acts as insulator.



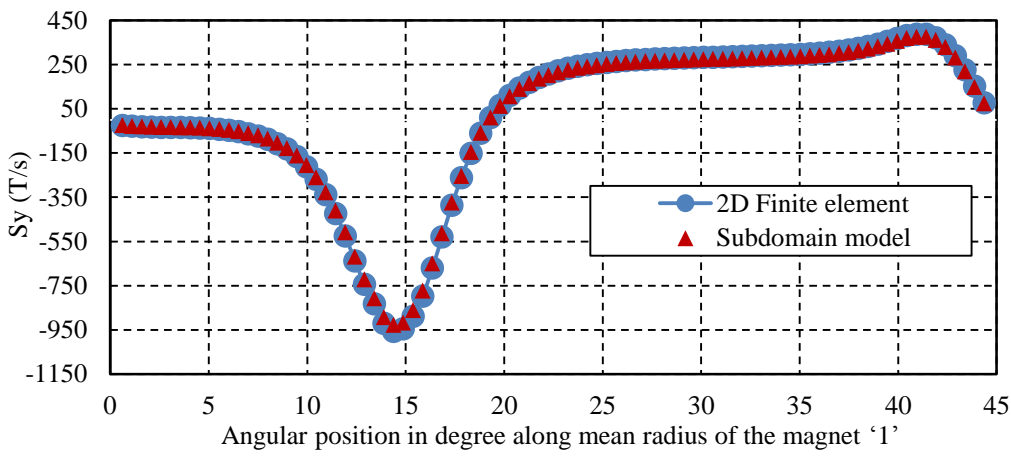
a



b



c



d

**Fig.3.** Comparison of source components from 2D FE and slotting effect model at mean radius of the magnet '1' at  $\omega_r t = 1.25^\circ$

- a Circumferential component -  $S_x$  (18-slot, 8-pole SPM)
- b Radial component -  $S_y$  (18-slot, 8-pole SPM)
- c Circumferential component -  $S_x$  (12-slot, 8-pole SPM)
- d Radial component -  $S_y$  (12-slot, 8-pole SPM)

Fig.4a compares the instantaneous loss computed for the first four magnets and their total when the 18-slot, 8-pole SPM machine is having 2 axial segments and no circumferential segments when excited at peak load conditions. The magnet loss is observed to be repeating at every  $1/6^{\text{th}}$  fundamental frequency[41], and hence the losses evaluation is repeated over this time span and averaged to predict the magnet loss. Fig.4b compares analytically and 3D FE predicted instantaneous total eddy current loss variations in 18-slot, 8-pole SPM with rotor position when the machine operates at the peak load condition with each magnet per pole segmented into 2 pieces axially. Fig.4c compares the analytically and 3D FE

predicted variations of z and x components of the current density with x in magnet '1' under the previously mentioned conditions.

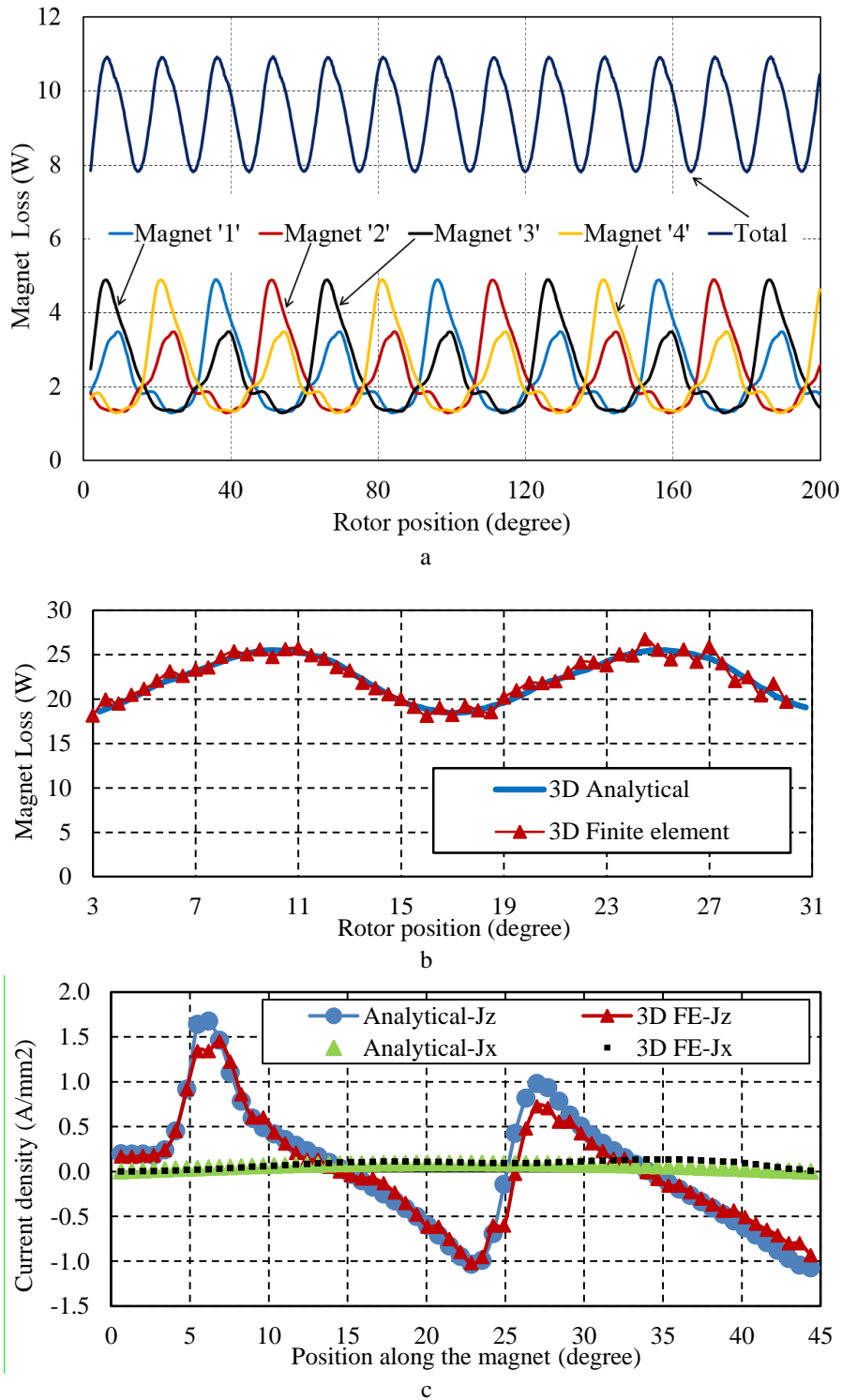
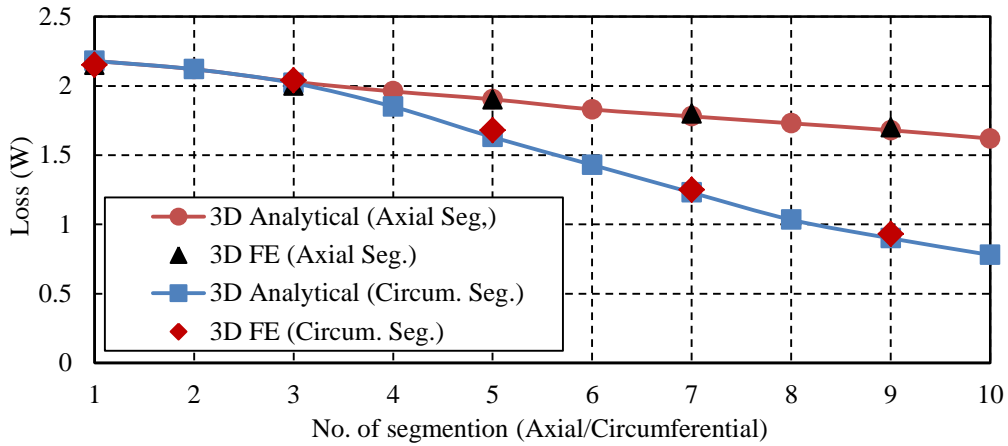


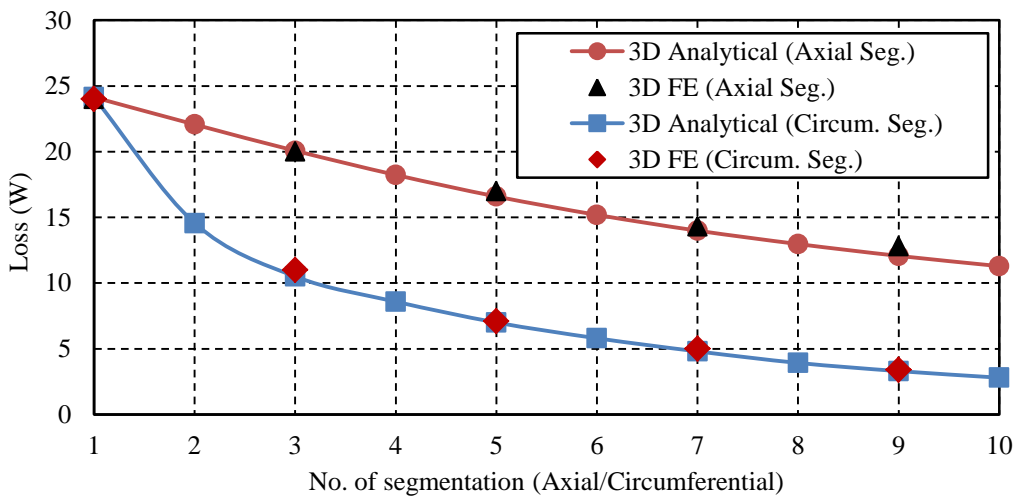
**Fig.4.** Instantaneous variation of magnet loss with rotor position for 18-slot, 8-pole SPM machine  
a Loss associated with magnets 1-4 and their total  
b Loss comparison from the proposed method and 3D FE  
c  $J_x$  and  $J_z$  comparison in magnet '1' ( $0 < x < L_x$ ) at  $\omega_r t = 4^\circ$ ,  $z = 0.75 L_z$  and  $y = 0.5 L_y$

Good agreement between the analytical and 3D FE predicted instantaneous values are observed albeit few minor mismatches which may be attributed to the curvature, the end winding effects and the core saturation which is neglected in the proposed method.

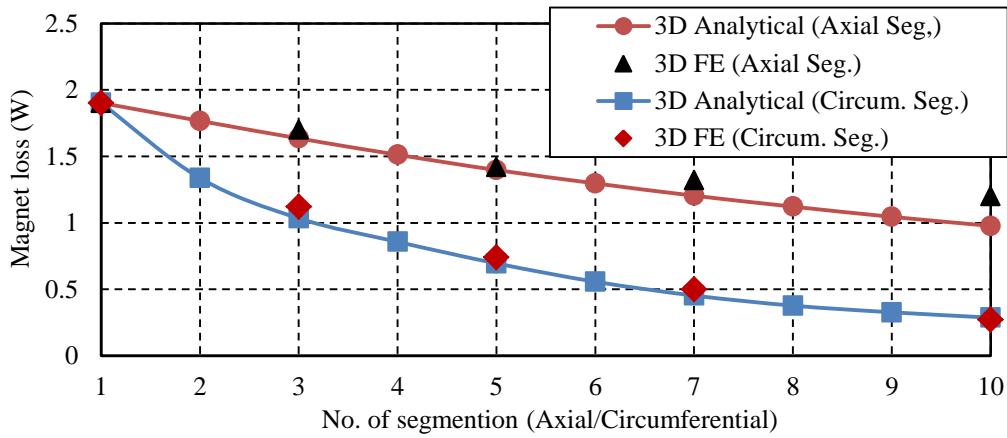
Fig.5 compares analytically and 3D FE predicted eddy current loss at no load and peak load with increase in axial and circumferential segmentation for both the SPM machines.



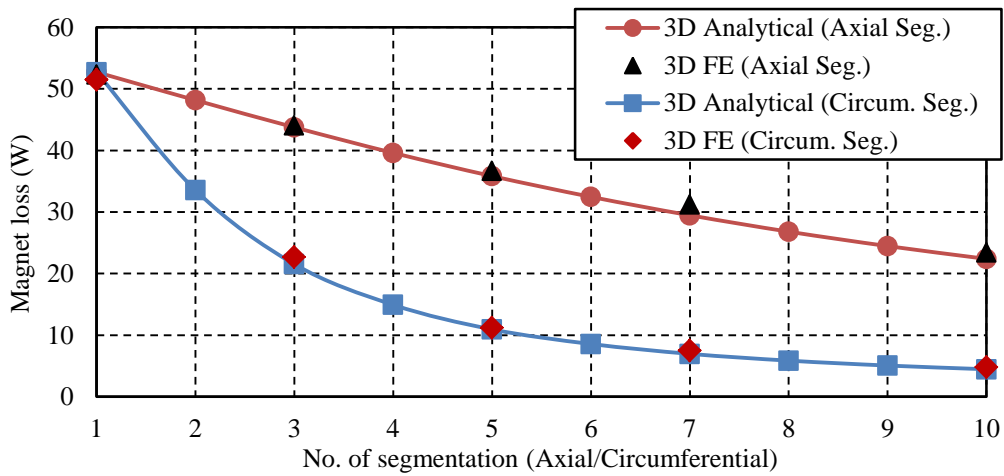
a



b



c



d

**Fig.5.** Magnet loss with increase in Axial and circumferential segmentation

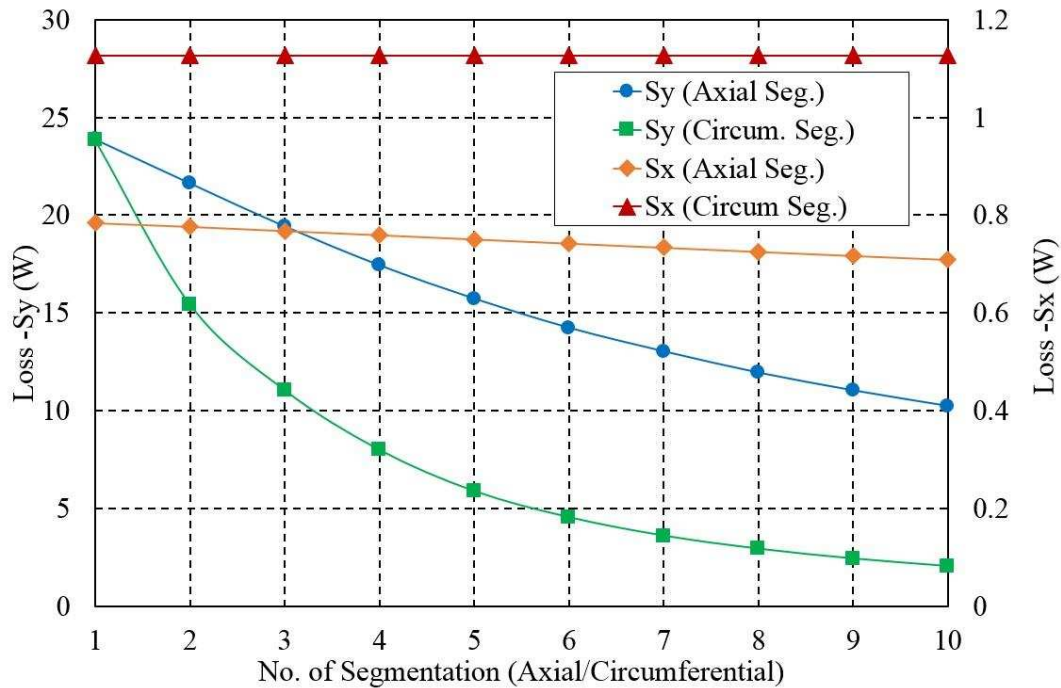
- a No load conditions for 18-slot, 8-pole SPM
- b Peak load conditions for 18-slot, 8-pole SPM
- c No load conditions for 12-slot, 8-pole SPM
- d Peak load conditions for 12-slot, 8-pole SPM

It can be seen that in all cases, good agreements are obtained between the 3D FE and analytical results. Also it can be seen that the no load loss is reduced with the 12-slot, 8-pole combination compared to the 18-slot, 8-pole machine as a result of reduction in the number of slots. However, the magnet loss at the same load conditions is found to be much higher in the 12-slot, 8-pole machine. This is because the 18-slot, 8-pole machine employs winding design features to reduce the space harmonics and hence the rotor eddy current loss [43], while retaining the merits of fractional slot per pole machine topology.

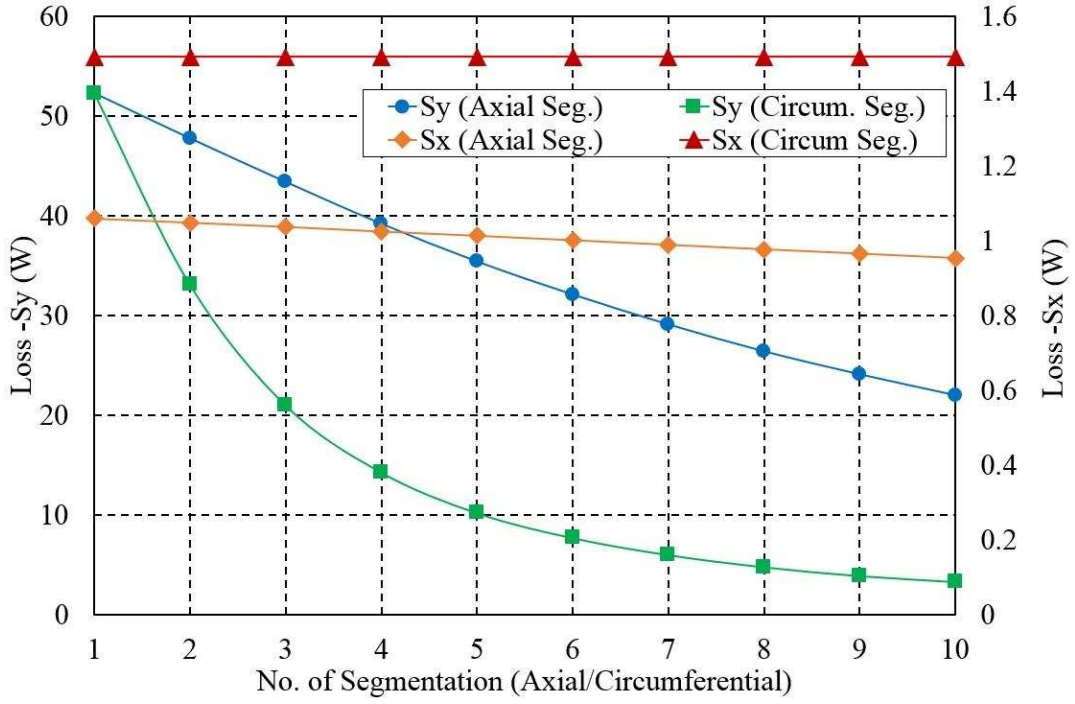
## 6. Evaluation of the results

### 6.1. Separation of magnet loss based on source components

Since the eddy current source within the PM has two components,  $\partial B_r/\partial t$  and  $\partial B_t/\partial t$ , it is insightful to assess the contribution of each towards the magnet loss. Fig. 6 shows the contribution of tangential and radial source components ( $S_x, S_y$ ) of flux density towards magnet loss, with increase in axial and circumferential number of segmentations when both the machine operates in the peak load conditions at 4500rpm. It is observed that the contribution of  $\partial B_t/\partial t$  towards the magnet loss is less significant, being an order of magnitude lower, compared to the loss contribution due to  $\partial B_r/\partial t$  at lower number of magnet segments. This is because the radial component of flux density,  $B_r$ , in a magnet is usually dominant, and hence both the rms and peak values of  $\partial B_r/\partial t$  are much greater than those of  $\partial B_t/\partial t$ , as is evident in Fig.3 whilst the resultant eddy current loss is proportional to square of the time derivatives.



a



b

**Fig.6.** Magnet loss associated with source components at peak load with increase in axial and circumferential segmentations  
a Loss associated with source components in 18-slot,8-pole SPM  
b Loss associated with source components in 12-slot,8-pole SPM

Further, the reduction of the loss associated with  $\partial B_t/\partial t$  is found to decrease very slowly with increase in the axial number of segments. Moreover, the loss associated with  $\partial B_t/\partial t$  is found to have no significant variation with the circumferential number of segments. This is because the eddy currents due to  $\partial B_t/\partial t$  flows in 2D y-z plane and segmentation along x- direction cannot alter the eddy current circulation path. It is also worth noting that the actual magnet loss in the machine is found to be lower than the sum of the losses due to the time derivatives of the radial and tangential flux density components as a result of harmonic interaction between the sources which can be seen from the definition of  $J_z$  in (8). The results follows that circumferential segmentation is not effective in reducing the eddy current loss associated with  $\partial B_t/\partial t$ .

## 6.2. Variation of harmonic loss with number of segmentations

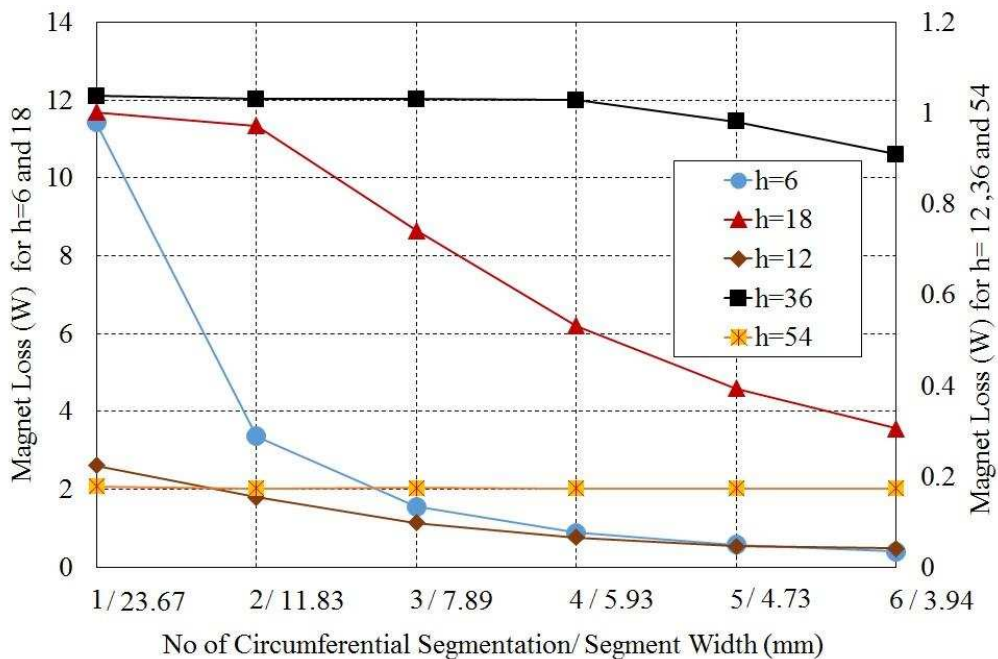
The analytical solution of source components given in (5), (6) allows to evaluate the different harmonic contents present in the eddy currents. It is observed that the harmonics which are resulting in loss in the rotor reference are of the orders  $(n_1 p_s + p)$  and  $(n_2 p_s - p)$  as identified in [13], where  $n_1 = 2, 5, 8, \dots$  and  $n_2 = 1, 4, 7, \dots$ ,  $p_s$  is the number of pole-pairs associated with the stator winding and  $p$  the rotor pole pairs.

The contribution of the forward and the reverse rotating harmonics of the same order towards the flux density variations is accounted together as they interact with each other [13] in loss production. These time harmonics are found to be of the order of 6, 12, 18, 24, 30, 36, 42, 48, 54...in 18-slot,8-pole SPM machine. It is observed from the loss computation that the major contributors for the magnet loss among them are of the orders 6, 12, 18, 36 and 54. The time harmonics are found to be of the order of 12, 24, 36, 48, 60...in 12-slot,8-pole SPM machine and the major contributors for the magnet loss among them are of the orders 12, 24, and 36.

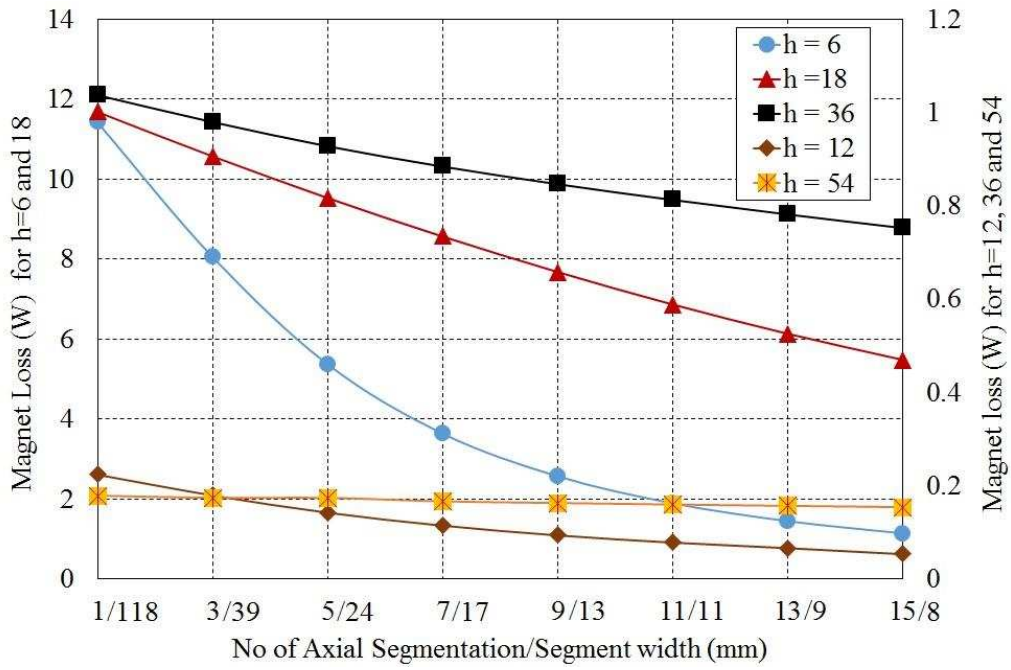
**TABLE 2** Wave length Associated with Major Harmonics

Harmonic No. (h)	6	12	18	24	36	54
Wavelength $\lambda_h$ (mm)	32.46	16.23	10.82	8.12	5.41	3.60

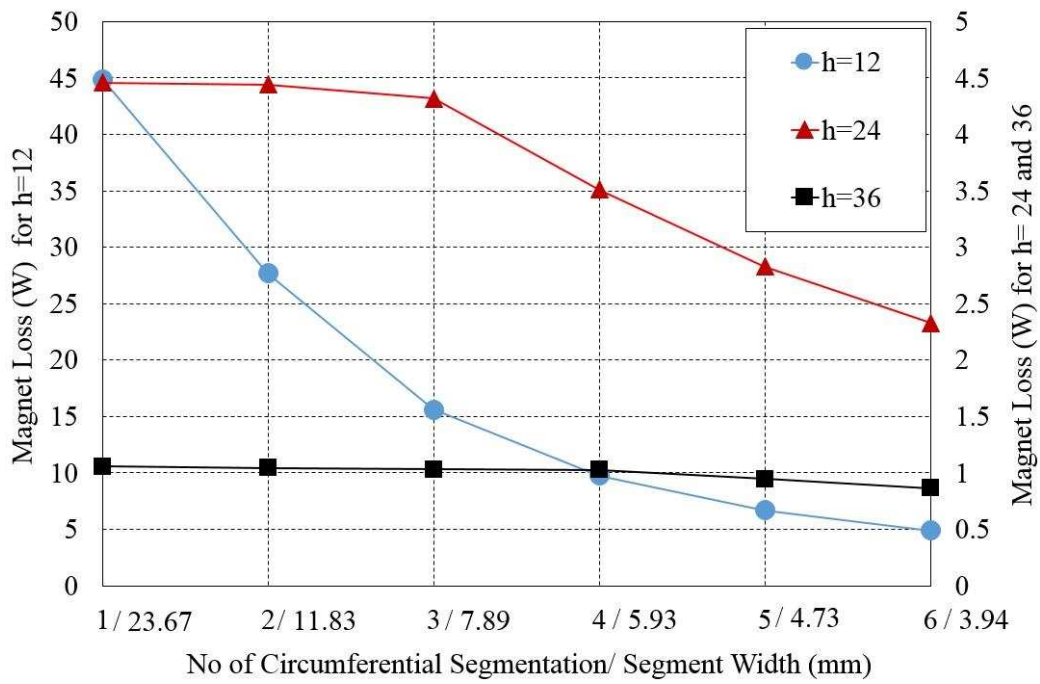
The wavelengths associated with these harmonics calculated based on the mean magnet radius (31mm) are tabulated in Table 2. The magnet loss variations for each major harmonic at peak load conditions with increase in circumferential and axial number of segments for the 18-slot,8-pole machine is compared in Figs. 7a and b respectively. For the purpose of illustration, the segment widths are also given for each number of segmentations.



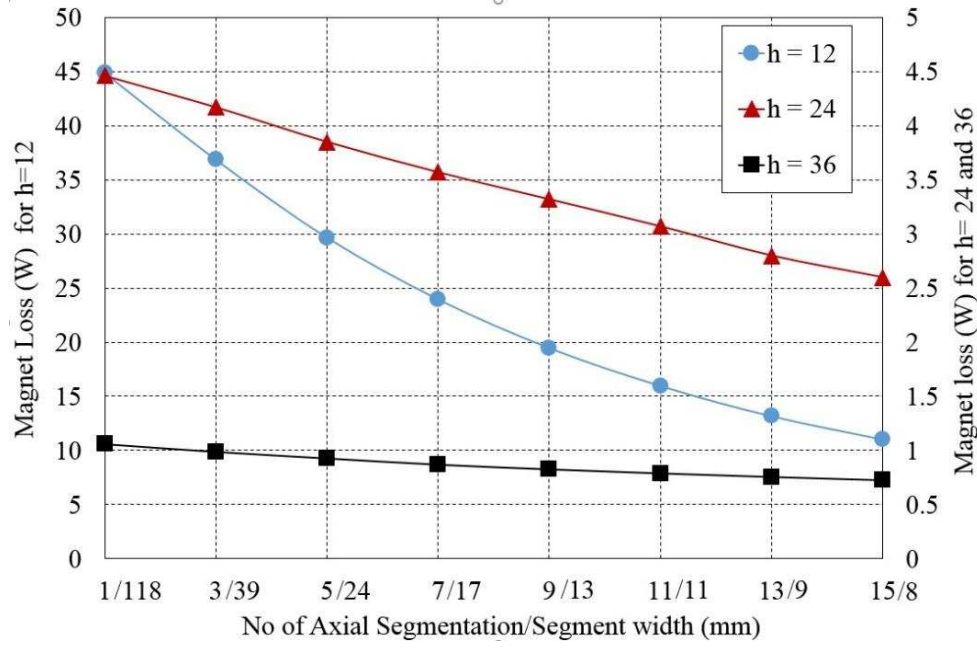
a



b



c



d

**Fig.7.** Comparison of loss variations associated with major harmonics at peak load with number of segments or with segment width

- a Circumferential segmentation in 18-slot, 8-pole SPM
- b Axial segmentation in 18-slot, 8-pole SPM
- c Circumferential segmentation in 12-slot, 8-pole SPM
- d Axial segmentation in 12-slot, 8-pole SPM

As can be seen, for the 18-slot,8-pole SPM the 6th and 18th harmonics contribute to ~94 % of the total magnet loss, where the loss contributions from 12, 36 and 54 orders of harmonics are shown in the scale of the secondary y-axis to clearly understand the relationship between the segment widths and the harmonic wavelengths.

Given that the circumferential segmentation is effective in reducing the eddy current loss associated with  $\partial B_r / \partial t$ , it is clear from Fig.7a that those harmonics most affected by the circumferential segmentation have their wavelength ( $\lambda_h$ ) greater than the circumferential segment width [38]. Hence magnet loss reduction by circumferential segmentation will be less effective when the harmonic wavelength ( $\lambda_h$ ) is lower than circumferential segment width, but becomes effective when the wavelength is greater than circumferential segment width. For example, the loss associated with the 18th harmonic is reduced at a faster rate when the number of circumferential segments are greater than two as the wavelength (10.82 mm) of the 18th harmonic becomes lower than the segment width (11.83 mm). For the case with the 6th harmonic, its wavelength (32.46 mm) is already lower than the segment width (23.67mm) when the number of circumferential segment is one, hence the associated loss is reduced at a faster rate with any further circumferential segmentations. However, it can be observed that the loss reduction

becomes slow with increase in circumferential number of segmentations when the harmonic wavelength is much greater than the segment width. The above phenomenon can be understood by the fact that when a harmonic wavelength is shorter than the segment width, the induced eddy current due to  $\partial B_r/\partial t$  which mainly circulates on the x-z plane can return easily within the segment. However, the eddy current return path is hampered when the segment width is shorter than the wavelength, resulting in a greater reduction in eddy current circulation and hence the associated loss.

For the case with axial segmentation it can be observed from Fig.7b that the rate of loss reduction with increase in number of segmentations decreases with increase in harmonic order. Hence the loss associated with the 6th harmonic is reduced at a much faster rate than that of the 54th harmonic (h=54) with increase in the axial number of segmentations. While the circumferential segmentation only affects the eddy current circulation due to  $\partial B_r/\partial t$ , the axial segmentation breaks both the induced eddy current paths due to  $\partial B_r/\partial t$  and  $\partial B_t/\partial t$ , and hence it is effective for reduction of eddy current losses associated with both the radial and circumferential components. The increase in the axial number of segments will increase the effective resistance of the z-component of the eddy current density, and hence reduces the eddy current losses. Thus, the axial segmentation will be effective in loss reduction even the wavelength of a harmonic is shorter than the axial segment height, as is evident from Fig. 7b. However, the harmonic loss reduction is observed at a slower pace with increase in axial segmentation number. This is because the magnet segment height is also reduced at a lower rate with increase in axial segmentation number.

From Figs.7c and d it can be seen that for the 12-slot, 8-pole SPM machine the loss the associated with the 12<sup>th</sup> harmonic is much higher compared to all other harmonics, resulting in the increased magnet loss. Also it is clear that the 12-slot, 8-pole SPM machine also follows the same trend for the harmonic loss variations with increase in circumferential and axial segmentations as observed previously for the 18-slot, 8-pole SPM machine.

Hence it may be preferred to segment the permanent magnet in the circumferential direction so that the width of the segment is lower than the wavelengths of all the dominant harmonics responsible for eddy current loss, followed by axial segmentation which targets those harmonics whose wavelengths is close or greater than the magnet width after the first step. However, segmentations in both directions have to be considered in the context of manufacturing feasibilities and cost.

## 7. Conclusions

A computationally efficient and accurate means for predicting 3D eddy current loss in rotor magnets of PM machines has been developed considering slotting based on 3D Fourier expansion of time-derivatives of flux density in magnets. The developed method has been validated by 3D FEAs on 18-slot,

8-pole and 12-slot,8-pole SPM machines. On an average for evaluating the loss variation with increase in axial number of segmentation up to 10, it takes around 2 minutes for each case, in contrast to more than 36 hours usually required for one 3D FE analysis with no axial segmentation on a typical 3.3 GHz, 64GB PC. It is observed that the loss contribution from the tangential component of the magnetic field variation is much lower in comparison to the loss associated with radial field variations. The method of axial segmentation is found to be better in reducing magnet loss from those harmonics with their wavelength lower than the segment width. The developed method provides an effective tool for assessing eddy current loss and for devising segmentation schemes for the loss reduction.

## 8. References

- 1 Lazari, P., Wang, J., Liang, C.: 'A Computationally Efficient Design Technique for Electric-Vehicle Traction Machines', *IEEE Trans. Ind. Appl.*, 2014, **50**, pp. 3203-3213
- 2 Atallah, K., Wang, J., Howe, D.: 'Torque-ripple minimization in modular permanent-magnet brushless machines', *IEEE Trans. Ind. Appl.*, 2003, **39**, pp. 1689-1695
- 3 Wrobel, R., Mellor, P.H.: 'Design Considerations of a Direct Drive Brushless Machine With Concentrated Windings', *IEEE Trans. Energy Convers.*, 2008, **23**, pp. 1-8
- 4 Zhou, P., Lin, D., Xiao, Y., Lambert, N., Rahman, M.A.: 'Temperature-Dependent Demagnetization Model of Permanent Magnets for Finite Element Analysis', *IEEE Trans. Magn.*, 2012, **48**, pp. 1031-1034
- 5 Sergeant, P., Van den Bossche, A.: 'Segmentation of Magnets to Reduce Losses in Permanent-Magnet Synchronous Machines', *IEEE Trans. Magn.*, 2008, **44**, pp. 4409-4412
- 6 Stoll, R.L., 'The analysis of eddy currents', (Clarendon Press, 1974)
- 7 Yoshida, K., Hita, Y., Kesamaru, K.: 'Eddy-current loss analysis in PM of surface-mounted-PM SM for electric vehicles', *IEEE Trans. Magn.*, 2000, **36**, pp. 1941-1944
- 8 Ruoho, S., Santa-Nokki, T., Kolehmainen, J., Arkkio, A.: 'Modeling Magnet Length In 2-D Finite-Element Analysis of Electric Machines', *IEEE Trans. Magn.*, 2009, **45**, pp. 3114-3120
- 9 Nannan, Z., Zhu, Z.Q., Weiguo, L.: 'Rotor Eddy Current Loss Calculation and Thermal Analysis of Permanent Magnet Motor and Generator', *IEEE Trans. Magn.*, 2011, **47**, pp. 4199-4202
- 10 Toda, H., Zhenping, X., Wang, J., Atallah, K., Howe, D.: 'Rotor eddy-current loss in permanent magnet brushless machines', *IEEE Trans. Magn.*, 2004, **40**, pp. 2104-2106
- 11 Zhu, Z.Q., Ng, K., Schofield, N., Howe, D.: 'Improved analytical modelling of rotor eddy current loss in brushless machines equipped with surface-mounted permanent magnets', *IEE Electr. Power Appl.*, 2004, **151**, pp. 641-650
- 12 Ishak, D., Zhu, Z.Q., Howe, D.: 'Eddy-current loss in the rotor magnets of permanent-magnet brushless machines having a fractional number of slots per pole', *IEEE Trans. Magn.*, 2005, **41**, pp. 2462-2469
- 13 Wang, J., Atallah, K., Chin, R., Arshad, W.M., Lendenmann, H.: 'Rotor Eddy-Current Loss in Permanent-Magnet Brushless AC Machines', *IEEE Trans. Magn.*, 2010, **46**, pp. 2701-2707
- 14 Rahideh, A., Korakianitis, T.: 'Analytical magnetic field distribution of slotless brushless permanent magnet motors - Part 1. Armature reaction field, inductance and rotor eddy current loss calculations', *Electric Power Applications, IET*, 2012, **6**, pp. 628-638
- 15 Dubas, F., Rahideh, A.: 'Two-Dimensional Analytical Permanent-Magnet Eddy-Current Loss Calculations in Slotless PMSM Equipped With Surface-Inset Magnets', *IEEE Trans. Magn.*, 2014, **50**, pp. 54-73
- 16 Bianchi, N., Bolognani, S., Fornasiero, E.: 'An Overview of Rotor Losses Determination in Three-Phase Fractional-Slot PM Machines', *IEEE Transactions on Industry Applications*, 2010, **46**, pp. 2338-2345
- 17 Bianchi, N., Fornasiero, E.: 'Impact of MMF Space Harmonic on Rotor Losses in Fractional-Slot Permanent-Magnet Machines', *IEEE Transactions on Energy Conversion*, 2009, **24**, pp. 323-328
- 18 Bianchi, N., Fornasiero, E.: 'Index of rotor losses in three-phase fractional-slot permanent magnet machines', *IET Electric Power Applications*, 2009, **3**, pp. 381-388
- 19 Wu, L.J., Zhu, Z.Q., Staton, D., Popescu, M., Hawkins, D.: 'Analytical Model for Predicting Magnet Loss of Surface-Mounted Permanent Magnet Machines Accounting for Slotting Effect and Load', *IEEE Trans. Magn.*, 2012, **48**, pp. 107-117
- 20 Zhu, Z.Q., Ng, K., Schofield, N., Howe, D.: 'Analytical prediction of rotor eddy current loss in brushless machines equipped with surface-mounted permanent magnets. I. Magnetostatic field model', in, *Proc. IEEE ICEM*, (2001)

- 21 Martin, F., Zaim, M.E.H., Tounzi, A., Bernard, N.: 'Improved Analytical Determination of Eddy Current Losses in Surface Mounted Permanent Magnets of Synchronous Machine', IEEE Trans. Magn., 2014, **50**, pp. 1-9
- 22 Fang, Z.X., Zhu, Z.Q., Wu, L.J., Xia, Z.P.: 'Simple and accurate analytical estimation of slotting effect on magnet loss in fractional-slot surface-mounted PM machines', in, Proc. IEEE ICEM, (2012)
- 23 Zarko, D., Ban, D., Lipo, T.A.: 'Analytical calculation of magnetic field distribution in the slotted air gap of a surface permanent-magnet motor using complex relative air-gap permeance', IEEE Trans. Magn., 2006, **42**, pp. 1828-1837
- 24 Zarko, D., Ban, D., Lipo, T.A.: 'Analytical Solution for Cogging Torque in Surface Permanent-Magnet Motors Using Conformal Mapping', IEEE Trans. Magn., 2008, **44**, pp. 52-65
- 25 Boughrara, K., Ibtouen, R., x, arko, D., Touhami, O., Rezzoug, A.: 'Magnetic Field Analysis of External Rotor Permanent-Magnet Synchronous Motors Using Conformal Mapping', IEEE Trans. Magn., 2010, **46**, pp. 3684-3693
- 26 Qazalbash, A.A., Sharkh, S.M., Irenji, N.T., Wills, R.G., Abusara, M.A.: 'Rotor eddy loss in high-speed permanent magnet synchronous generators', Electric Power Applications, IET, 2015, **9**, pp. 370-376
- 27 Zhu, Z.Q., Wu, L.J., Xia, Z.P.: 'An Accurate Subdomain Model for Magnetic Field Computation in Slotted Surface-Mounted Permanent-Magnet Machines', IEEE Trans. Magn., 2010, **46**, pp. 1100-1115
- 28 Lubin, T., Mezani, S., Rezzoug, A.: '2-D Exact Analytical Model for Surface-Mounted Permanent-Magnet Motors With Semi-Closed Slots', IEEE Trans. Magn., 2011, **47**, pp. 479-492
- 29 Wu, L.J., Zhu, Z.Q., Staton, D., Popescu, M., Hawkins, D.: 'Analytical prediction of electromagnetic performance of surface-mounted PM machines based on subdomain model accounting for tooth-tips', Electric Power Applications, IET, 2011, **5**, pp. 597-609
- 30 Wu, L.J., Zhu, Z.Q., Staton, D., Popescu, M., Hawkins, D.: 'Analytical Modeling and Analysis of Open-Circuit Magnet Loss in Surface-Mounted Permanent-Magnet Machines', IEEE Trans. Magn., 2012, **48**, pp. 1234-1247
- 31 Wang, J., Papini, F., Chin, R., Arshad, W.M., Lendenmann, H.: 'Computationally efficient approaches for evaluation of rotor eddy current loss in permanent magnet brushless machines', in, Proc. IEEE ICEM, (2009)
- 32 Okitsu, T., Matsushashi, D., Muramatsu, K.: 'Method for Evaluating the Eddy Current Loss of a Permanent Magnet in a PM Motor Driven by an Inverter Power Supply Using Coupled 2-D and 3-D Finite Element Analyses', IEEE Trans. Magn., 2009, **45**, pp. 4574-4577
- 33 Yamazaki, K., Shina, M., Kanou, Y., Miwa, M., Hagiwara, J.: 'Effect of Eddy Current Loss Reduction by Segmentation of Magnets in Synchronous Motors: Difference Between Interior and Surface Types', IEEE Trans. Magn., 2009, **45**, pp. 4756-4759
- 34 Mirzaei, M., Binder, A., Deak, C.: '3D analysis of circumferential and axial segmentation effect on magnet eddy current losses in permanent magnet synchronous machines with concentrated windings', in, Proc. IEEE ICEM, (2010)
- 35 Mirzaei, M., Binder, A., Funieru, B., Susic, M.: 'Analytical Calculations of Induced Eddy Currents Losses in the Magnets of Surface Mounted PM Machines With Consideration of Circumferential and Axial Segmentation Effects', IEEE Trans. Magn., 2012, **48**, pp. 4831-4841
- 36 Okitsu, T., Matsushashi, D., Yanhui, G., Muramatsu, K.: 'Coupled 2-D and 3-D Eddy Current Analyses for Evaluating Eddy Current Loss of a Permanent Magnet in Surface PM Motors', IEEE Trans. Magn., 2012, **48**, pp. 3100-3103
- 37 Peng, Z., Sizov, G.Y., Jiangbiao, H., Ionel, D.M., Demerdash, N.A.O.: 'Calculation of magnet losses in concentrated-winding permanent magnet synchronous machines using a Computationally Efficient - Finite Element method', in, Energy Conversion Congress and Exposition (ECCE), 2012 IEEE, (2012)
- 38 Aslan, B., Semail, E., Legranger, J.: 'General Analytical Model of Magnet Average Eddy-Current Volume Losses for Comparison of Multiphase PM Machines With Concentrated Winding', IEEE Trans. Energy Convers., 2014, **29**, pp. 72-83
- 39 Masmoudi, A., Masmoudi, A.: '3-D Analytical Model With the End Effect Dedicated to the Prediction of PM Eddy-Current Loss in FSPMMs', IEEE Trans. Magn., 2015, **51**, pp. 1-11
- 40 Pyrhonen, J., Jussila, H., Alexandrova, Y., Rafajdus, P., Nerg, J.: 'Harmonic Loss Calculation in Rotor Surface Permanent Magnets- ;New Analytic Approach', IEEE Trans. Magn., 2012, **48**, pp. 2358-2366
- 41 Chen, L., Wang, J., Nair, S.S.: 'An analytical method for predicting 3D eddy current loss in permanent magnet machines based on generalized image theory', IEEE Trans. Magn., 2015, **PP**, pp. 1-1
- 42 Nair, S., Wang, J., Chen, L., Chin, R., Manolas, I., Svehkarenko, D.: 'Prediction of 3D High Frequency Eddy Current Loss in Rotor Magnets of SPM Machines', IEEE Transactions on Magnetics, 2016, **PP**, pp. 1-1
- 43 Wang, J., Patel, V.I., Weiya, W.: 'Fractional-Slot Permanent Magnet Brushless Machines with Low Space Harmonic Contents', IEEE Trans. Magn., 2014, **50**, pp. 1-9

## 9. Appendix

### 9.1. Definition of $abr$ , $afr$ , $\psi br$ , $\psi fr$ , $aba$ , $afa$ , $\psi ba$ , $\psi fa$ , in evaluating $S_x$ and $S_y$

$\mathbf{a}_{br} = \left  -\mathbf{a}_{1l}e^{j\psi_{al}} - \mathbf{c}_{1l}e^{j(\psi_{cl}-\frac{\pi}{2})} \right /2$	$\mathbf{a}_{b\alpha} = \left  -\mathbf{a}_{1l}e^{j(\psi_{al}-\frac{\pi}{2})} + \mathbf{c}_{1l}e^{j\psi_{cl}} \right /2$
$\mathbf{a}_{fr} = \left  -\mathbf{a}_{1l}e^{-j\psi_{al}} + \mathbf{c}_{1l}e^{-j(\psi_{cl}-\frac{\pi}{2})} \right /2$	$\mathbf{a}_{f\alpha} = \left  \mathbf{a}_{1l}e^{-j(\psi_{al}-\frac{\pi}{2})} + \mathbf{c}_{1l}e^{-j\psi_{cl}} \right /2$
$\psi_{br} = \text{angle} \left( -\mathbf{a}_{1l}e^{j\psi_{al}} - \mathbf{c}_{1l}e^{j(\psi_{cl}-\frac{\pi}{2})} \right)$	$\psi_{b\alpha} = \text{angle} \left( -\mathbf{a}_{1l}e^{j(\psi_{al}-\frac{\pi}{2})} + \mathbf{c}_{1l}e^{j\psi_{cl}} \right)$
$\psi_{fr} = \text{angle} \left( -\mathbf{a}_{1l}e^{-j\psi_{al}} + \mathbf{c}_{1l}e^{-j(\psi_{cl}-\frac{\pi}{2})} \right)$	$\psi_{f\alpha} = \text{angle} \left( \mathbf{a}_{1l}e^{-j(\psi_{al}-\frac{\pi}{2})} + \mathbf{c}_{1l}e^{-j\psi_{cl}} \right)$

## 9.2. Solutions to the Eddy Current Functions

The coefficients,  $c(m,n,k)$ ,  $d(m,n,k)$ ,  $e(m,n,k)$ ,  $h(m,n,k)$ ,  $q(m,n,k)$  for the current vector potential and eddy current densities, and  $p1(m,n,k)$  -  $p5(m,n,k)$  for the eddy current loss are defined as follows:

$$\text{Let } M^2 = \left(m \frac{\pi}{L_x}\right)^2 + \left(n \frac{\pi}{L_y}\right)^2 + \left(k \frac{\pi}{L_z}\right)^2 \quad (22)$$

$$c_{(m,n,k)} = \sigma \cdot \frac{a_{(m,n,k)}}{M^2} \quad (23)$$

$$d_{(m,n,k)} = \sigma \cdot \frac{b_{(m,n,k)}}{M^2} \quad (24)$$

$$e_{(m,n,k)} = \sigma \cdot \frac{-b_{(m,n,k)} \left(k \frac{\pi}{L_z}\right)}{M^2} \quad (25)$$

$$h_{(m,n,k)} = \sigma \cdot \frac{a_{(m,n,k)} \left(k \frac{\pi}{L_z}\right)}{M^2} \quad (26)$$

$$q_{1(m,n,k)} = \sigma \cdot \frac{b_{(m,n,k)} \left(m \frac{\pi}{L_x}\right)}{M^2} \quad (27)$$

$$q_{2(m,n,k)} = \sigma \cdot \frac{-a_{(m,n,k)} \left(n \frac{\pi}{L_y}\right)}{M^2} \quad (28)$$

$$p_{1(m,n,k)} = b_{(m,n,k)}^2 \cdot \left[ \frac{\left(k \frac{\pi}{L_z}\right)^2}{M^2} \right] \cdot \frac{\sigma L_x L_y L_z}{8} \quad (29)$$

$$p_{2(m,n,k)} = a_{(m,n,k)}^2 \cdot \left[ \frac{\left(k \frac{\pi}{L_z}\right)^2}{M^2} \right] \cdot \frac{\sigma L_x L_y L_z}{8} \quad (30)$$

$$p_{3(m,n,k)} = b_{(m,n,k)}^2 \cdot \left[ \frac{\left(m \frac{\pi}{L_x}\right)^2}{M^2} \right] \cdot \frac{\sigma L_x L_y L_z}{8} \quad (31)$$

$$p_{4(m,n,k)} = a_{(m,n,k)}^2 \cdot \left[ \frac{\left(n \frac{\pi}{L_y}\right)^2}{M^2} \right] \cdot \frac{\sigma L_x L_y L_z}{8} \quad (32)$$

$$p_{5(m,n,k)} = -2a_{(m,n,k)}b_{(m,n,k)} \cdot \left(m \frac{\pi}{L_x}\right) \left(n \frac{\pi}{L_y}\right) \cdot \left[\frac{1}{M^2}\right]^2 \cdot \frac{\sigma L_x L_y L_z}{8} \quad (33)$$